Improved Estimation Methods for Lead Acid Utility Arrays for Microgrids

Christopher R. Lashway, *Student Member*, Osama Mohammed, *Fellow, IEEE*
Energy Systems Research Laboratory, 10555 West Flagler St, Engineering Center 3983, Miami, FL, 33174

***Abstract*—In this paper, an enhanced mathematical model is introduced for accurately estimating the injection (charging) and extraction (discharging) of current from a lead acid cell and is extended to a much broader scale for use in utility energy storage applications. A comprehensive analysis is conducted on a common lead acid cell model to interpret it in terms of a normalization metric accurately forecasting the energy transfer based on the current state-of-charge (SoC) level. Discharge and charge models are created where normalized parameters are used in conjunction with the published capacity of the battery (in Ah) to obtain the charging and discharging currents. Particular focus is placed on the nonlinearity present in the constant voltage and float charging regions where a 3rd order polynomial model is used. The charging algorithm is further capable of identifying a drift in the published full charging current as a battery ages to adjust the cutoff condition. An experimental verification is conducted on a 12 Ah 3-cell lead acid battery depicting the usage of the proposed algorithm can accurately estimate the battery behavior.**

***Index Terms*—Lead-Acid Batteries, Modelling, state-of-charge (SOC), Battery Capacity**

I. Introduction

The lead acid battery still remains one of the oldest electrochemical energy storage devices in use today. The most common usage remains in the automotive field where it remains in a float-charge stage for most of its lifespan, primarily utilized for the in-rush current required to turn over a starter. Unfortunately, with the introduction of new electric vehicles (EV), the effects of deep discharge and high currents have a significant consequence on their lifespan. The utilization of these batteries in EVs has recently been investigated, but remains limited due to state-of-health (SoH) impacts [1].

Despite its susceptibility to capacity-loss and sulfation through continuous use and exposure to high currents, the lead acid cell has a simple construction and its materials remain inexpensive. In a much broader scale such as that of a utility array, it is currently feasible to deploy lead acid in bulk and the tactic is nothing new [2]. In [3], the usage of lead acid batteries for utility applications is analyzed in terms of their economic viability and advantages for spinning reserves, load following, frequency control, and peak shaving. As their usage in utility applications continues to grow, so does the need to accurately forecast their behavior.

The most challenging aspect in effective utilization of lead acid is minimization of the charging time. The constant current phase of lead acid charging only accounts for approximately 60% of the process, where the remaining nonlinear portions take a significant amount of time [4]. In [5], a study was conducted in an attempt to improve the speed of charging in EV applications through experimenting with pulsed charging. Through the usage of short duration pulses between 100 ms and 600 ms, a charging scheme was able to inject more energy into the battery in a shorter period of time but it required an amplitude of 85%-115% of the battery capacity.

Charging is heavily burdened by electrochemical properties where the injection current is constrained with respect to the current state of charge (SoC). Without accounting for this aspect, one can significantly misjudge the duration and energy absorbed during a charging period. This case is particularly frequent when investigating the behaviors of a complex hybrid power system where the energy input can be misjudged as a linear function into and out of the lead acid array [6],[7].

The nonlinear characteristics of the charging curve are typically modeled using a simple exponential, but this does not tell the full story and does not have the capability to depict unique features which can occur past 100% state-of-charge (SoC) [5]. Some work has been carried out to improve estimations in this region but most have been limited to indirect approaches. In [8], a back propagation neural network is used to approximate the behavior of a high-capacity lead acid charging model. High precision was achieved in the process but the algorithm is computationally intensive.

In this paper, an algebraic approach is taken with respect to the practical usage of the lead acid battery in an energy storage array. A comprehensive analysis is conducted on a common lead acid cell model to interpret it in terms of a normalized set of parameters to predict the current into and out of the battery at a given SoC level. Discharge and charge models are created based on the ampere-hour size of any lead acid battery. The model is tested with a comparison to a 12 Ah uninterruptible power system (UPS) battery to depict the accuracy.

This paper is organized as follows: the common lead acid battery electrochemical and Thevenin circuit model is discussed in Section II. Section III discusses the need and method to capacity-based normalization of the charging and discharging process. Section IV demonstrates an experimental

verification of the battery model whereas section V concludes the study.

II. Common Lead Acid Battery Modeling

The history of the lead acid cell can be dated back to well over a century. The development of the first secondary battery traces back to 1859 by French physicist Gaston Planté, but has followed clearly followed a series of improvements [4]. The common lead acid battery employed in-practice today follows the use of lead and lead dioxide for the cathode and anode. This combined with an electrolyte interface consisting of sulfuric acid and water provides a catalyst for electrochemical energy to be generated. The chemical formula defining the total reaction is defined in (1) where the lead and lead dioxide electrodes are placed in a combination of sulfuric acid to generate electrons to supply a load.

$$\mathrm{Pb} + \mathrm{PbO_2} + 2\mathrm{H_2SO_4} + 2e^- \rightleftharpoons 2\mathrm{PbSO_4} + 2\mathrm{H_2O} + 2e^- \quad (1)$$

Moving from the left-hand side of the chemical equation, one can define the charging process. From a 100% state-of-charge (SoC), a mix of sulfuric acid and water (H_2SO_4) reaches a saturation point where the electrolyte has a concentration ratio of approximately 60% sulfuric acid and 40% water. The result is shown at the right-hand side of the equation where the discharging process terminates and the electrolyte is composed of virtually all water molecules.

A. Thevinen Model

A basic acceptable model depicting a battery is shown in Fig. 1 [9]. This simplified model identifies 3 major parameters that can be witnessed experimentally where an internal resistance parameter is accounted for prior to a charging and discharging circuit each with their own unique resistive components.

What is typically neglected in this model is that all resistors are variable and depend on a range of different factors. The simplest and most common is the battery internal resistance which for a new battery would remain constant but would adjust over time with respect to usage characteristics, age, and other state-of-health (SoH) effects. The modeled discharge and charge parameters, however, also have very different nonlinear characteristics as well and are discussed in the following sections.

The Thevinen equivalent circuit equation based on the SoC is shown in (1) where $R_c(\lambda)$ and $R_{dc}(\Lambda)$ represent lumped

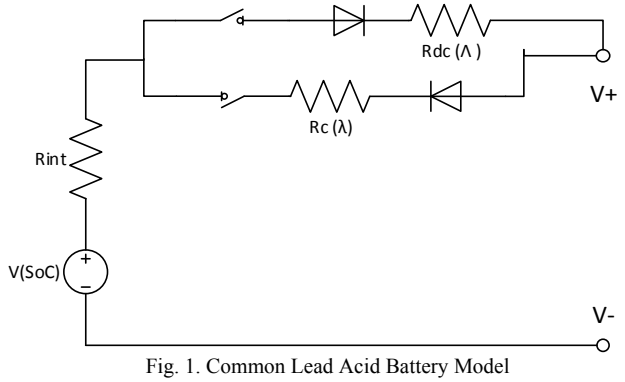

Fig. 1. Common Lead Acid Battery Model

parameters designating the charge and discharge resistance, respectively. The usage of ideal diodes are placed to indicate a case of charging and discharging concurrently is impossible and thus the voltage drop is not accounted for in (2).

$$V(SoC) = \begin{cases} [R_{int}(t) + R_c(\lambda)]I(t) & \text{charging} \\ [R_{int}(t) + R_{dc}(\Lambda)]I(t) & \text{discharging} \end{cases} \quad (2)$$

B. Charging Constraints

One of the most complicated processes in lead acid battery operation is the proper charging. From the previous section, it was established that charging involved the utilization of electrons to alter the electrolyte concentration [10]. As the concentration changes, a generation of sulfuric acid occurs where molecules of sulfuric acid absorb electrons. This stage, known as constant current, in an ideal case can absorb an infinite number of electrons at virtually any level of current. However, charging current is typically limited as thermodynamic and mechanical stress to the battery increases significantly as the charging rate increases.

Assuming a charging current limited to C/20 or the 20-hour charging rate, the absorption of electrons into the electrolyte begins to saturate as the voltage of the cell rises to meet that of the charger. This area refers to the constant voltage charging phase as the saturation of the electrolyte begins to prevent charge injection thereby limiting current. As the battery reaches the charger voltage, the current will begin to drop logarithmically until it reaches a steady-state known as the full charge current. The full charge current is typically identified as 3% of the rated C20 current level. .

C. Discharging Constraints

Discharging is governed much more different than that of charging. Virtually any discharge current can be applied but as each current is increased past the C20-rate, the available energy will reduce nonlinearly. Although there are a number of components that are involved to model the activation energies impacting the discharge resistance $R_{dc}(\Lambda)$ in (2), modeling a microgrid case can be simplified through employing Peukert's component. This method is especially useful in a grid configuration where a control and estimation system for a large array of batteries would operate best by limiting the computational analysis but requires a dimensionless factor designating the exponential decay of energy as the current is adjusted.

Under a C20-rate this function would expect to be linear, however this would not be realistic with respect to the type of loads applied from the grid. Although there would be an expected wide range of load profiles produced on the DC side, for the sake of analysis these loads can be expected to be resistive. The inclusion of a constant current discharge condition is not realistic in the sense of energy utilization. For this reason, the output waveform is modeled as a resistance with an output current variance equal to the voltage variation of the cell.

D. SOC-Based Energy Extraction/Injection

The objective of this work is to use the constraints governing the charging and discharging process to obtain a time invariant model where a control system can use a SoC value to determine the reasonable current that could be extracted or injected into a lead acid battery. This model is intended to help improve estimations used in simulations and develop control systems which can forecast the charging and load flow when applied directly to a lead acid array. This array structure begins through the analysis and development of a mathematical function modeling the behavior of a single lead-acid cell model for two reasons:

- Normalizing the charge injection should be performed on a single cell first in order to not omit crucial details and phenomena of electrochemistry;
- Common design considerations and battery management systems in utility arrays following NEC 480.1 have established that utility arrays usually control at the cell level [11].

In conjunction with single-cell modeling identifies a need to also produce a normalized parameter of the energy extracted and injected into the battery. Once a normalized parameter has been established, this value can be used in conjunction with the rated capacity of the battery to obtain a value of current that can be calculated for virtually any battery.

III. Capacity-Based Normalization

Charging and discharging rates must be optimized for usage in a microgrid application. In many cases, the discharging rate can be misrepresented as being unlimited or at a level which is far above the 20-hour (C20) discharging rate. In this paper, the discharging rate is targeted for the C20 rate to maximize battery efficiency and charge transfer. The charging scheme, however, operates very differently. By applying the same C20 charging current, electrochemical saturation effects occurring above the 60% SoC level will significantly limit the current injection and cause this period to last well beyond 20 hours. To battle these effects, the charging current is increased to a 10-hour rate (C10).

The C10 rate, as shown later in Fig. 2, yields a total charging time of approximately 12 hours. Through the use of these two metrics, the final charging and discharging equations are written in the form of a fraction of the amp-hour capacity of the battery. The normalized model can then hereby predict the current rate of virtually any lead acid capacity where the total rated capacity of the cell E_{tot} is divided by 20 to obtain to 20-hour discharge current and 10 to obtain the maximum charging current.

$$I_{dc_{C20}} = \frac{E_{tot}}{20} = 0.05E_{tot} \quad (3)$$

$$I_{c_{C10}} = \frac{E_{tot}}{10} = 0.10E_{tot} \quad (4)$$

This work was partially supported by grants for the Office of Naval Research.
The authors are with the Energy Systems Research Laboratory, Department of Electrical and Computer Engineering, Florida International University, Miami, FL 33174 (e-mail: mohammed@fiu.edu).

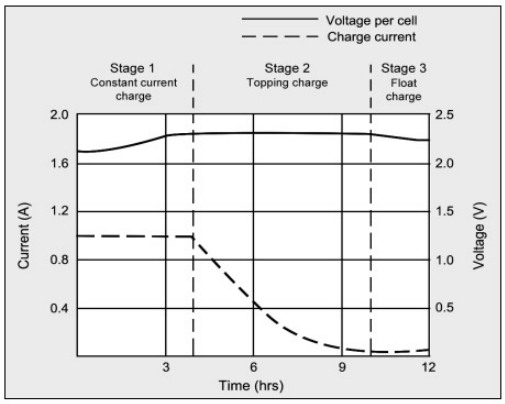

Fig. 2. Lead Acid Cell Charging Mode at 1 A Max [12]

A. Normalized Charging Model

A normalized charging curve for a single lead acid cell is shown in Fig. 2 [12]. This model identifies a standard charging scheme of a single lead-acid cell where an initial constant current at C10 is applied. The cell voltage is shown in solid line and current in the dashed line. By inspection, the charging voltage variation from 0% SoC to 100% SoC is minimal. The crucial factor is the charging current, which depicts a maximum constant current limit of 1 A which progresses into the highly nonlinear constant voltage and float charge phases. During the constant voltage phase, an exponential fall-off occurs leading into the float charge phase.

The float charging phase will typically begin to saturate near a full charging current. This point is initially defined as 8% of the 20-hour discharge current. However, a closer inspection to Fig. 2 reveals a characteristic that can normally go unnoticed. As the battery progresses from constant voltage to float charging, it will reach a local minima unique to that particular charge cycle. If the charging continues past its cutoff current, injection of current into the battery would eventually reach a knee and later, begin to increase. This feature is a crucial element that many models neglect due to the nature of the increase in current being so small. For a new battery, this phenomenon is irrelevant as the battery would be expected to simply reach a full charging current and immediately shut down the charger. However, as the battery begins to age, the battery will reach a point where it is unable to reach the published full charge current. In this case, the knee of this curve becomes a crucial characteristic in preventing overcharge.

Developing an adequate model for the nonlinear portion of the charging curve has been performed using the MATLAB Curve Fitting toolbox. A number of different functions were attempted with respect to the waveform shown in Fig. 2. Of the various functions tested, the Fourier and Polynomial-based models produced the lowest root mean squared error (RMSE) calculations. Fourier models had RMSE values of 2.68% and 1.52% for 1st and 2nd-ordered sets. The 3rd order polynomial produced an RMSE of 2.60% and was ultimately selected for the nonlinear portion of the model shown in Fig. 3. Although a 2nd-order Fourier model produced a smaller RMSE, the 3rd

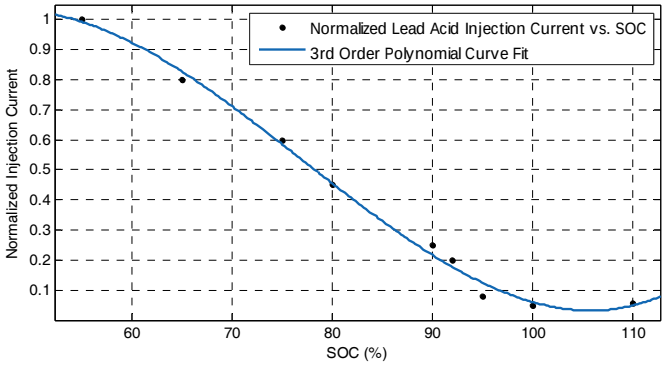

Fig. 3. Constant Voltage & Float Charge Curve Fit

order polynomial provides the closest approximation into accurately modeling the float charging phase cycle. The float charging cutoff is modeled in Fig. 3 by extending the SoC beyond its 0-100% range to indicate the behavior of the current in an overcharge case. The best equation depicting a normalized charging model with respect to the SoC (S) is:

$$\mathrm{I_c} = \begin{cases} 1, & S \le 60\% \\ [0.01S^3 - 2.4S^2 + 162S - 2200] \times 10^{-3}, & S > 60\% \end{cases} \quad (5)$$

Equation (5) is then adjusted to constrain the maximum current to a C10 rate as depicted in (4). Equation (5) is then becomes:

$$\mathrm{I_{c_{C10}}} = \begin{cases} 0.1E_{tot}, & S \le 60\% \\ E_{tot}[0.01S^3 - 2.4S^2 + 162S - 2200]10^{-4}, & S > 60\% \end{cases} \quad (6)$$

B. Normalized Discharging Model

The normalized discharging model applies similar constraints as to that of the charging section, except discharging is not limited by electron absorption and saturation as that of charging. The discharging of a lead acid cell is assumed to be regulated at the 20-hour discharge rate as indicated in Equation (3) where a modification is applied based on practical operation of the cell.

During typical operation, it is not reasonable to assume the output current would remain constant at the C20 rate. Although it is also unlikely that the resistance would remain constant across the load, this case is more realistic in the case of a utility array. For this reason, the closest approximation or the loading on the discharging side is modeled as an average 20-hour discharge resistance rather than a current. To obtain this, a correction factor must be implemented to govern the variance of the current extraction from the cell as it progresses from 100% to 0% SoC.

The current extraction model is adjusted with respect to the voltage variance where $V_{100\%}$ indicates the voltage of the cell at full charge and $V_{0\%}$ is the voltage under load at full discharge. The cell voltages use published electrode potential values where $V_{100\%}$ and $V_{0\%}$ are 2.10 V and 1.75 V respectively [12]. The voltage variance, ΔV is thus 0.35 V or approximately 16% between 0% and 100% SoC. This indicates that by placing a resistance value consistent with the voltage at 50%

TABLE I
UB 6120 12 AH LEAD ACID BATTERY SPECIFICATIONS

Nominal Voltage	7 V
Capacity	12 Ah
C20 Discharge Current	0.6 A
C10 Charging Current	1.2 A
Published Full Charge Cutoff	18 mA
Actual Full Charge Cutoff	127 mA

SoC, the variance would be balance ±8% from full charge state to full discharge state. The final normalized function with respect to the battery capacity, E_{tot} is thus:

$$I_{dc_{C20}} = -0.05E_{tot}[1 - 0.0016S] \quad (7)$$

C. Final Normalized Model

The final normalized model is shown above in Fig. 4. The bounds have been extended beyond the usable battery range to identify the overcharge region. Any amp-hour capacity value can be substituted for E_{tot} to obtain the local charge and discharge currents with respect to the current SoC. The following section will present 2 case studies to test this model against a 3-cell lead acid battery.

IV. EXPERIMENTAL TEST RESULTS

In order to validate this model, the UB 6120 3-cell UB 6120 12-Ah lead acid battery used in the experimental test [13]. The UB 6120 specifications are shown below in Table I. To conduct the battery cycling, a battery test stand was developed using the LabVIEW Development Platform. A 9.5Ω resistive load is implemented where the center C20 current at 50% SoC is equal to approximately 0.6 A. A controlled power supply is used as a source regulated to a maximum C10 current, or 1.2 A. The normalized cycle profile in Fig. 4 is adjusted to conform to the expected charging and discharging currents of the 12 Ah battery capacity.

The experimental test analyzes a new UB 6120 battery under the normal C20 discharging constraints and a maximum C10 charging profile. The charging profile is extended past 100% SoC to depict the knee of the curve corresponding to Equation (6). The empirical charging and discharging curves are shown in Fig. 5. Fig. 6 demonstrates the close relationship

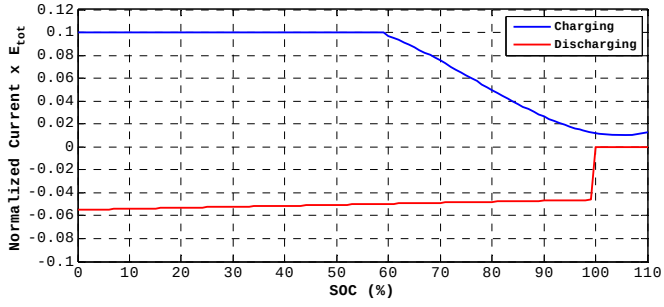

Fig. 4. Normalized Current versus SoC Model Based on Battery Capacity

to that of the mathematical model as the experimental results are superimposed over that of the mathematical model. These results follow a close trend but do not depict as much of a rise in the current once the system has reached 10% of overcharge displayed in Fig. 7.

The float charge component in Equation (6) was useful in determining the actual 100% SoC cutoff. Unfortunately, it required the overcharging of the battery by approximately 10% to depict the curve trend. As shown in Table I, the "Published Full Charge Cutoff" is 3% of the C20 current, or 18 mA. The actual full charge cutoff identified experimentally was 7 times higher. This would have been left unidentified and allowed the battery to continue into overcharge without ever reaching 18 mA. Through utilizing the nonlinear portion of the charging model, this could have been avoided. A closer view of this fit is displayed in Fig. 7. The nonlinear portion identified the local minima of 127 mA where a minor increase of current following this curve indicated to the control system that the battery had reached a full charging current. Through the application of this algorithm, an overcharge case would have been prevented and an accurate estimation would have been provided to a utility control system.

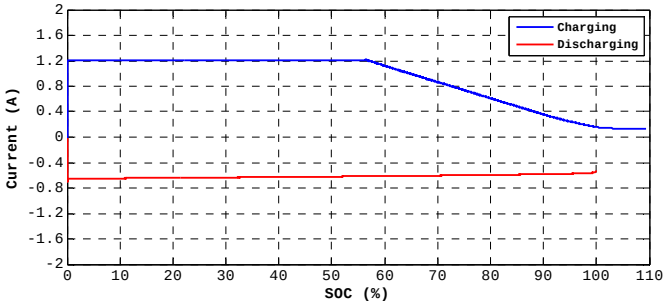

Fig. 5. Experimental Cycling Data from UB 6120

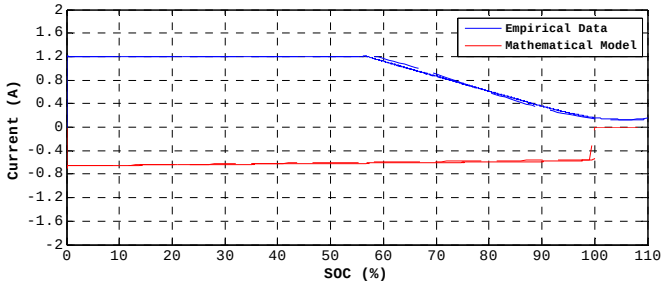

Fig. 6. Experimental versus Mathematical Model

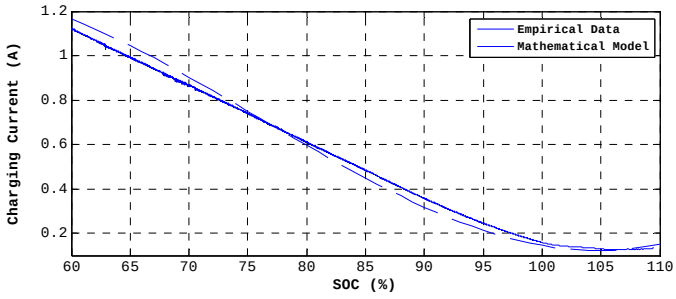

Fig. 7. Nonlinear Charging Equation Portion versus Experimental Data

V. Conclusion

This paper provides an overview of the electrochemical constraints present in the common lead acid battery and provides an improved, advanced mathematical model to determine the amount of current that can be charged or discharged from a lead acid cell based simply upon the state of charge. A lead-acid cell voltage versus current model is analyzed and its current profile is normalized for usage in a lead acid battery of virtually any capacity. Normalized charging and discharging curves are developed based simply on the ampere-hour rating on the faceplate of the lead acid battery. The discharging profile is modeled based in a utilization of a constant resistive load tuned to maximize capacity output and minimize cell damage. The charging current is modeled to minimize damage while still inject current at a higher rate than what has been discharged. Critical characteristics depicting the constant voltage and float charge phases of the charging curve are modeled using a 3rd order polynomial which further compensates for the drift in a published full charge current by identifying a local minima. The results depict a strong correlation between the experimental results versus the mathematical model where a published full charge current is unattainable. Through the application of this algorithm, a utility or vehicle control system can accurately estimate the current transfer into and out of a lead acid battery bank with respect to the current state of charge.

References

[1] B. S. Bhangu, P. Bentley, D. . Stone, and C. M. Bingham, "State-of charge and state-of-health prediction of lead-acid batteries for hybrid electric vehicles using non-linear observers," in 2005 European Conference on Power Electronics and Applications, 2005, p. 10 pp.–P.10.

[2] J. Szymborski, G. Hunt, and R. Jungst, "Examination of VRLA battery cells sampled from the Metlakatla battery energy storage system," in The Sixteenth Annual Battery Conference on Applications and Advances, 2001, pp. 131–138.

[3] M. D. Anderson and D. S. Carr, "Battery energy storage technologies," Proceedings of the IEEE, vol. 81, no. 3, pp. 475–479, Mar. 1993.

[4] D. Linden, T. B. Reddy, "Lead Acid Batteries" in *Handbook of Batteries*, 3rd ed. New York, NY: McGraw-Hill, 2002, ch, 23.

[5] L. Siguang, Z. Chengning, and X. Shaobo, "Research on Fast Charge Method for Lead-Acid Electric Vehicle Batteries," in *International Workshop on Intelligent Systems and Applications, 2009. ISA 2009*, 2009, pp. 1–5.

[6] Chen, S.X.; Gooi, H.B.; Wang, M. Q., "Sizing of Energy Storage for Microgrids," *Smart Grid, IEEE Transactions on* , vol.3, no.1, pp.142,151, March 2012

[7] Lin Xu; Xinbo Ruan; Chengxiong Mao; Buhan Zhang; Yi Luo, "An Improved Optimal Sizing Method for Wind-Solar-Battery Hybrid Power System," *Sustainable Energy, IEEE Transactions on* , vol.4, no.3, pp.774,785, July 2013

[8] K. Yang, G. Ouyang, P. Zhang, and J. Zhang, "Research upon the high-capacity lead-acid battery charge model," in International Conference on Mechatronics and Automation, 2009. ICMA 2009, 2009, pp. 5079–5083.

[9] D. Maksimovic, "Lead-acid batteries" University of Colorado, Boulder, CO, 2014.

[10] R. S. Treptow, "The Lead-Acid Battery: Its Voltage in Theory and in Practice," J. Chem. Educ., vol. 79, no. 3, p. 334, Mar. 2002.

[11] M. W. Earley, J. S. Sargent, "Storage Batteries" in *National Electric Code 2011 Handbook*, 12th ed. Quincy, MA: National Fire Protection Association, 2010, ch. 4, sec. 480.

[12] Battery University, "Charging Lead Acid", Cadex, Richmond, BC, 2014.

[13] UPG, "Universal UB6120 TOY 6V 12 Ah SLA Battery Spec Sheet," UPG No. D5737, Carrollton, TX.